

Article

Study on the Properties and Hydration Mechanism of Calcium Carbide Residue-Based Low-Carbon Cementitious Materials

Qing Wang^{1,2,3}, Ying Wang^{1,2,3}, Xiaowei Gu^{1,2,3,*}, Jianping Liu⁴ and Xiaochuan Xu^{1,2,3}¹ School of Resources and Civil Engineering, Northeastern University, Shenyang 110819, China² Liaoning Institute of Technological Innovation in Solid Waste Utilization, Northeastern University, Shenyang 110819, China³ Science and Technology Innovation Center of Smart Water and Resource Environment, Northeastern University, Shenyang 110819, China⁴ Architectural and Civil Engineering College, Shenyang University of Technology, Shenyang 110027, China

* Correspondence: guxiaowei@mail.neu.edu.cn

Abstract: Alkali-activated cementitious materials, as an environmentally friendly cementitious material, can effectively reduce carbon emissions and improve the utilisation of solid wastes. However, traditional strong alkali activators have limitations such as high carbon emissions and poor safety. In order to overcome the defects of traditional strong alkaline activators and realise the high value-added use of calcium carbide residue (CCR), this paper adopts CCR as an alkaline activator to activate granulated blast furnace slag (GBFS)-steel slag (SS) cementitious systems for the preparation of alkaline-activated cementitious materials. The effects of CCR content and SS content on the compressive strength and working performance of CCR-GBFS-SS cementitious systems are analysed, along with the hydration process of CCR-GBFS-SS cementitious systems and the mechanism of action through the hydration products, their chemical structure and their microscopic morphology. The research results show that CCR-GBFS-SS cementitious systems have a 28-day compressive strength of 41.5 MPa and they can be controlled by the setting time; however, the flow performance is poor. The SS content can be increased to improve the flow performance; however, this will reduce the compressive strength. In CCR-GBFS-SS cementitious systems, CCR is the main driving force of hydration reactions, GBFS mainly provides active silica and aluminium and the amorphous C-(A)-S-H gel and ettringite formed by the synergistic action of multiple solid wastes are the main sources of compressive strength. With the extension of the curing time, the amount of hydration products in the cementitious systems gradually increases and the matrix of the cementitious systems gradually becomes denser. This study will provide a reference for the consumption of low-value solid waste such as CCR and the preparation of low-carbon cementitious materials from multi-component solid wastes.

Keywords: calcium carbide residue; granulated blast furnace slag-steel slag cementitious systems; compressive strength; workability; hydration process



Citation: Wang, Q.; Wang, Y.; Gu, X.; Liu, J.; Xu, X. Study on the Properties and Hydration Mechanism of Calcium Carbide Residue-Based Low-Carbon Cementitious Materials. *Buildings* **2024**, *14*, 1259. <https://doi.org/10.3390/buildings14051259>

Academic Editor: Haoxin Li

Received: 26 January 2024

Revised: 25 February 2024

Accepted: 4 March 2024

Published: 30 April 2024



Copyright: © 2024 by the authors. Licensee MDPI, Basel, Switzerland. This article is an open access article distributed under the terms and conditions of the Creative Commons Attribution (CC BY) license (<https://creativecommons.org/licenses/by/4.0/>).

1. Introduction

The production process of Portland cement, consisting of two grinding and one burning operations, produces a lot of CO₂ and pollutes the environment; thus, it is of great practical significance to develop green and low-carbon cementitious materials to replace Portland cement [1]. Among them, alkali-activated cementitious materials have similar properties to those of Portland cement, have environmentally friendly and energy-saving properties and are the most likely cementitious materials to replace Portland cement among various new building materials [2–4]. In the preparation of traditional alkali-activated cementitious materials, NaOH, Na₂SiO₄ and other strong alkalis are used as alkaline activators [5,6]. However, the setting time of cementitious materials under the activation of strong alkali activators is short and difficult to control, the process is expensive, and

other problems limit the use of alkali-activated cementitious materials [7,8]. Therefore, the use of activators with a relatively low alkalinity instead of strong alkaline activators is of significant research value.

Meanwhile, in China, more than 30 million tonnes of calcium carbide residue (CCR) is discharged annually, accumulating mostly in the open air, occupying a large amount of land resources and polluting the environment. The pH of CCR reaches 12.13, and the high alkalinity of CCR permits the use of CCR as an alkaline activator for the preparation of alkali-activated cementitious materials. Zhang et al. [9] used CCR and granulated blast furnace slag (GBFS) to prepare low-carbon cementitious materials; the results of their study showed that CCR can effectively promote the hydration of GBFS and that the hydration products of CCR-GBFS cementitious systems are mainly C-S-H gel, hydrotalcite and semicarboxate. Dueramae et al. [10,11] used CCR to activate fly ash and found that the compressive strength of CCR-fly ash cementitious systems was low and that the addition of an activator or an increase in the curing temperature could effectively improve the compressive strength of the cementitious systems. Guo et al. [12,13] prepared quaternary cementitious systems with different strengths (15–40 MPa) by using soda residue and CCR according to a certain ratio as a composite activator to simulate GBFS-fly ash cementitious systems. On the other hand, there is a large amount of accumulated steel slag (SS) in China, and although researchers have used SS in fields such as soil remediation catalysis, its high hardness, the difficulty of grinding it and its instability limit its application. There is still about 70 million tonnes of SS produced in China every year [14] that cannot be effectively utilised, so the use of SS in the preparation of cementitious materials is of great research value for the large-scale consumption of SS. Because of the low cementitious activity of SS, SS is often compounded with GBFS to prepare GBFS-SS alkali-activated cementitious materials. Zhao et al. [15] used GBFS-SS as the main precursor for the preparation of alkaline-activated cementitious materials, with NaOH as an activator, showing that the early hydration of SS will increase the pH of the pore solution of cementitious systems and promote the dissolution of the vitreous in GBFS. At the same time, the consumption of $\text{Ca}(\text{OH})_2$ in the pozzolanic reaction in the cementitious systems will promote the further hydration of SS. Zhong et al. [16–18] prepared clinker-free GBFS-SS alkali-activated cementitious materials using Na_2SiO_4 as an alkaline activator, and the results showed that the incorporation of SS reduced the total exothermic capacity of the cementitious systems. Most of the crystalline phases of SS did not participate in the hydration reaction, and the drying shrinkage of the cementitious systems was comparable to that of Portland cement with a low risk of alkali aggregate reactions when the SS content reached 40%.

At present, strong alkalis such as NaOH are still the most common activators for GBFS-SS cementitious systems; however, the performance and hydration characteristics of GBFS-SS cementitious systems under the activation of CCR have not been systematically investigated. Therefore, in order to enhance the utilisation of bulk, low-value, solid CCR and SS waste, in this paper, alkali-activated cementitious materials were prepared with CCR, SS and GBFS as the main raw materials. A small amount of gypsum (GY) was added as the sulphate activator to provide the necessary sulphate radical for the cementitious systems. The effects of the contents of CCR and SS on the compressive strength and working performance of the multi-solid waste cementitious systems were emphatically discussed. The hydration products and hydration process of the CCR-GBFS-SS cementitious systems were determined via XRD and other detection methods. This study can reduce the environmental pollution caused by industrial solid wastes such as CCR and SS, promote the transformation of harmful solid wastes into value-added resources, provide a reference for the preparation of multi-element, solid-waste, low-carbon cementitious systems and lay the foundation for the continuous optimization of CCR-GBFS-SS cementitious systems.

2. Test Materials and Methods

2.1. Raw Materials

The main raw materials used in this paper are CCR, SS, GBFS, GY and water. Among these, CCR and SS were taken from Zhengzhou City, Henan Province, China. S95 GBFS was taken from Shijiazhuang City, Hebei Province, China. GY is a pure analytical reagent of $\text{CaSO}_4 \cdot 2\text{H}_2\text{O}$ produced by Tianjin Zhiyuan, China. The specific components of the raw materials are shown in Table 1; the XRD spectra and particle size distribution are shown in Figure 1.

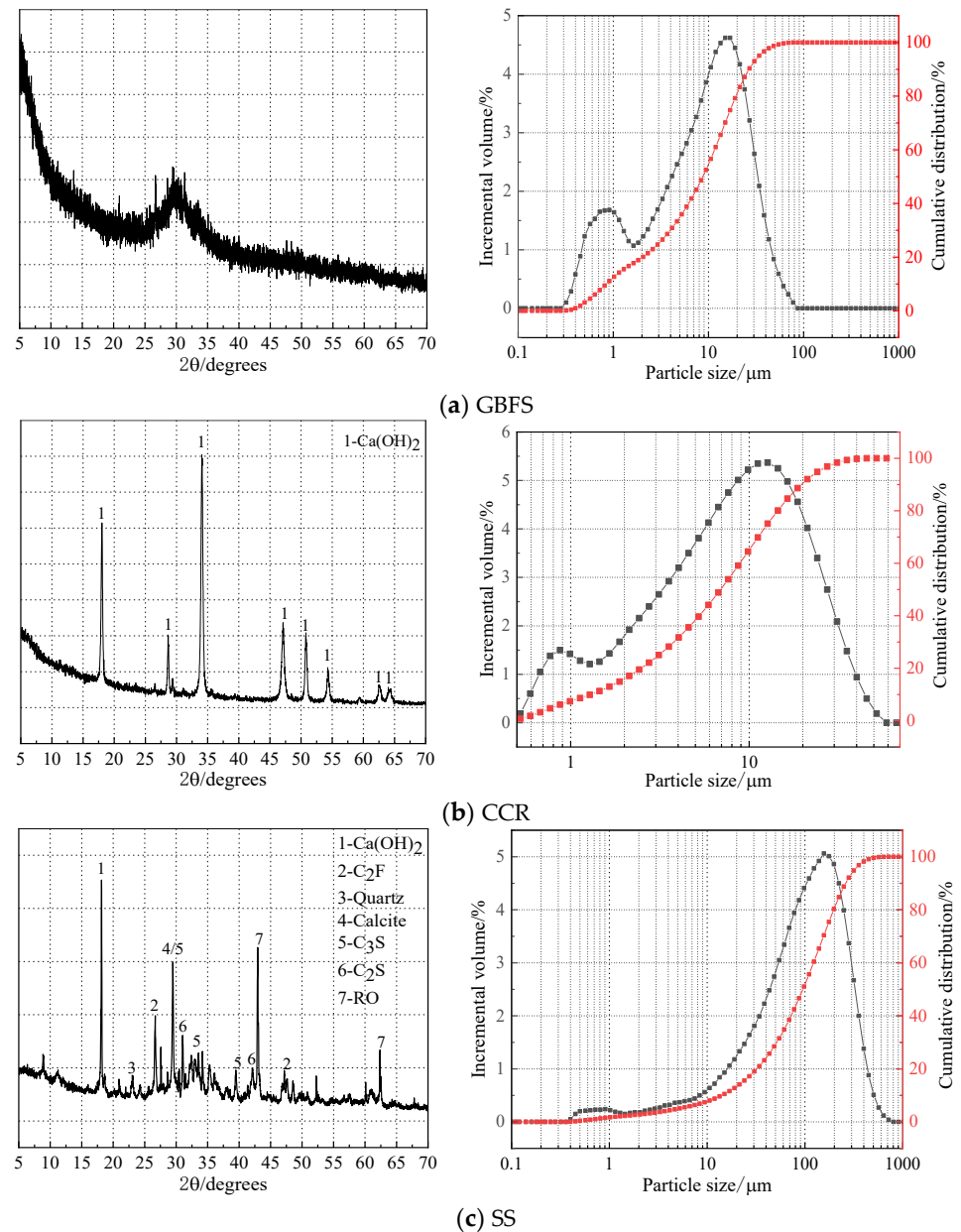


Figure 1. XRD and particle size of raw materials.

Table 1. Chemical composition of raw materials (%).

Ingredient	SiO_2	Al_2O_3	Fe_2O_3	MgO	CaO
CCR	7.68	3.96	0.2	0.79	85.23
SS	15.24	6.35	28.12	6.6	39.35
GBFS	34.50	17.70	1.03	6.01	34.00

CCR is a white powder; its main component is $\text{Ca}(\text{OH})_2$, with a $\text{Ca}(\text{OH})_2$ content of more than 90% and a water content of 0.7%. After mechanical grinding, the particle size of CCR is mainly 1–100 μm , and the D50 is 6.64 μm . SS is a grey-black powder, and its composition is more complex. It contains mainly C_3S , C_2S , $\text{Ca}(\text{OH})_2$, C_2F , quartz and the RO phase (MgO , FeO , MnO). SS is hard and difficult to grind; its particle size is mainly distributed in the range of 10–600 μm and the D50 of the SS used in this experiment is 95.28 μm . GBFS powder is made of iron ore blast furnace slag quenched by water into a granular ground powder; the S95 grade is a milky white powder and its main component is calcium aluminium xanthate feldspar (C_2AS). In the GBFS XRD spectrum at 25–35° degrees, there is an obvious hump, indicating that the GBFS powder contains a large number of glassy silica and aluminium components. The particle size of GBFS is mainly distributed between 1 and 100 μm , and the D50 is 8.75 μm .

2.2. Test Methods

2.2.1. Preparation for Specimens

On the basis of a large number of pre-experiments, the effect of CCR on the compressive strength of the cementitious systems was first analysed within a reasonable range. Then, cementitious systems with the optimal amount of CCR were selected, and the effect of the SS content on the compressive strength of cementitious materials was determined. Firstly, CCR, SS, GBFS and GY were mixed in a tank in the chosen proportions and stirred (140 rpm) for 180 s. Secondly, water was added, and the mixture was stirred (140 rpm) for 300 s and then poured into a 40 mm × 40 mm × 40 mm Sanlian mould. Finally, the moulds containing cementitious material were put into a curing cabinet with a curing temperature of $20\text{ }^\circ\text{C} \pm 2\text{ }^\circ\text{C}$ for 24 h for demoulding. After demoulding, the cementitious material was cured in a curing cabinet for 3 days, 7 days and 28 days and then submitted to compressive strength tests and microscopic analyses. The specific proportion of cementitious materials is shown in Table 2, and the preparation process is shown in Figure 2.

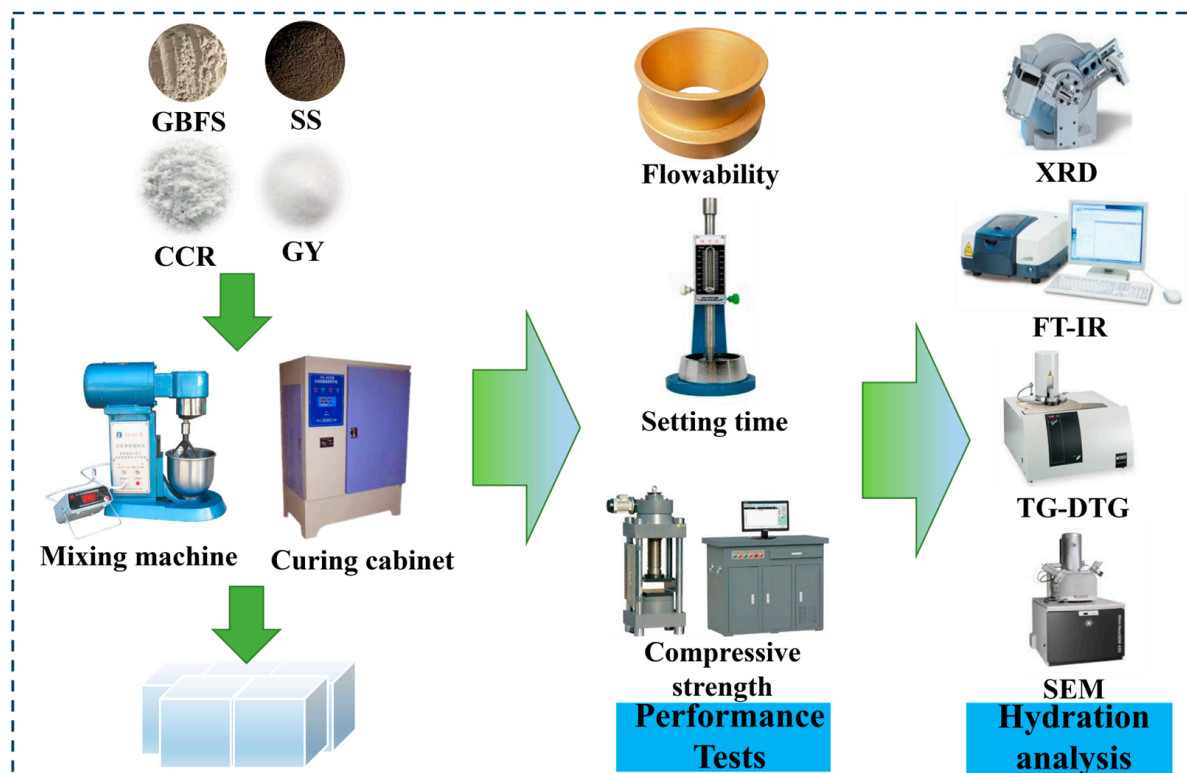


Figure 2. Test flow chart of cementitious material.

Table 2. Test mix ratio of cementitious material.

	CCR/g	SS/g	GBFS/g	GY/g	Water/g
T1	36	36	270	18	126
T2	54	36	252	18	126
T3	72	36	234	18	126
T4	54	72	216	18	126
T5	54	108	180	18	126

2.2.2. Flowability and Setting Time

This study evaluated the flowability of fresh paste using the fluidity test prescribed in the Chinese standard GB/T 8077-2012 [19,20]. The water/binder ratio of the paste was 0.5, and the test was conducted using a truncated cone mould made of copper with an upper opening diameter of 36 mm, a lower opening diameter of 60 mm and a height of 60 mm. Vicat apparatus was employed to measure the setting times, and the measurement was performed in accordance with the Chinese standard GB/T 1346-2011 [21,22]. It is crucial to note that after each measurement, the specimens were placed back into the curing box at $20\text{ }^{\circ}\text{C} \pm 2\text{ }^{\circ}\text{C}$.

2.2.3. Compressive Strength

The compressive strength was determined using the TSY-2000A testing equipment and the loading speed was 2.4 kN/s. The samples were tested for compressive strength at 3, 7 and 28 days of curing. The experimental procedure was conducted in accordance with the Chinese standard GB/T 17671-2021 [23,24].

2.2.4. Hydration Analysis

The test pieces cured for 3 days, 7 days and 28 days were further broken, and the central pieces were placed in anhydrous ethanol for 24 h to stop hydration. Before the test, the pieces were taken out and dried in a drying box at $40\text{ }^{\circ}\text{C}$ for 24 h, and small pieces with flat upper and lower surfaces were selected for SEM-EDS analysis and observation. The remaining pieces were ground to below 0.075 mm with agate mortar and analysed via XRD, FT-IR and TG-DTG.

2.2.5. Microscopic Testing Instrument

The hydration products of the cementitious systems were tested by XRD. The X-ray diffractometer (XRD) model is a Rigaku Dmax Ultima +, the manufacturer is Rigaku Corporation, Tokyo, Japan. the scanning range of 2θ was $5\text{--}70^{\circ}$ and the scanning rate was $10^{\circ}/\text{min}$. The chemical bond characteristics of hydration products were analysed via FT-IR with a Thermo Scientific Nicolet iS20, the manufacturer is Thermo Fisher Scientific, Bedford, MA, USA, and a wavenumber range of $400\text{--}4000\text{ cm}^{-1}$. The micro-morphology was analysed via a scanning electron microscope (SEM), and the model used was a Tescan Miralms, the manufacturer is TESCAN Brno, Brno-Kohoutovice, Czech. The hydration product and its water content were studied via a high-temperature thermal analyser. The model used was a Netzsch STA 449 F3, the manufacturer is Netzsch, Hanau, Germany. The test temperature was $30\text{--}1000\text{ }^{\circ}\text{C}$ and the heating rate was $20\text{ }^{\circ}\text{C}/\text{min}$.

3. Results and Analysis

3.1. Flowability of Fresh Paste in Cementitious Systems

Figure 3 shows the flowability of the cementitious systems of CCR-GBFS-SS with different amounts of CCR and SS. In Figure 3, the overall fluidity performance of the CCR-GBFS-SS cementitious systems is low. With the increasing content of CCR, the fluidity of the cementitious systems was 131 mm, 119 mm and 105 mm, showing a gradual decrease. When the content CCR is 20%, the fluidity is 19.8% lower than when the content of CCR is 10%, mainly because the main component of CCR is $\text{Ca}(\text{OH})_2$. $\text{Ca}(\text{OH})_2$ easily generates

holes, pits and other microstructures due to the loose crystal structure and the electrostatic effect, resulting in the CCR particles coming into complete contact with the surface of the water film and further increasing the water requirement of cementitious systems [25]. With an increasing content of SS, the fluidity of the cementitious systems is 119 mm, 139 mm and 154 mm, showing a gradual upward trend. When the content of SS is 30%, the flowability increases by 29.4% compared with that when the content of SS is 10%. The main reason for this is that the addition of SS reduces the amount of GBFS and the water demand of the cementitious systems. On the other hand, the low activity and large particle size of SS, in addition to a small specific surface area, mainly play the role of an “aggregate filling” in the paste to alleviate the close stacking and adsorption bonding of CCR and GBFS into clusters, which can reduce the cohesion and friction between the powders and improve the mobility performance of the cementitious systems.

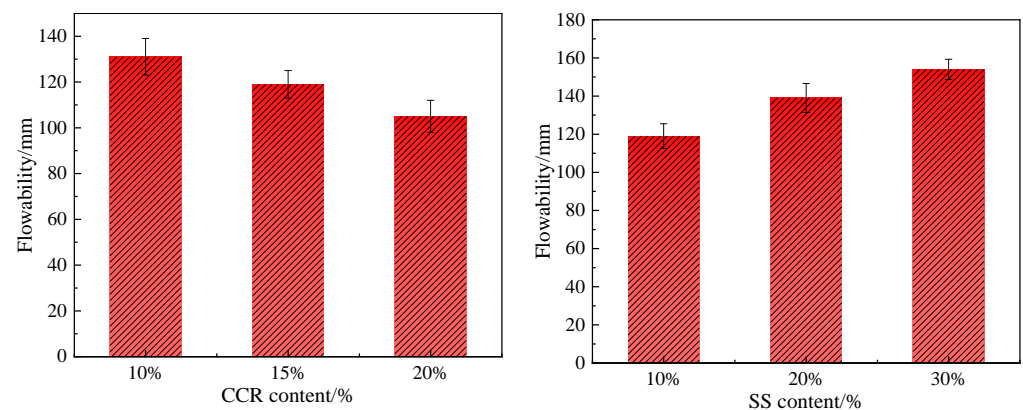


Figure 3. Flowability of cementitious systems with different material contents.

3.2. Setting Time of Fresh Paste in Cementitious Systems

Figure 4 shows the setting time of the cementitious systems with different contents of CCR and SS. In Figure 4, with the increasing amount of CCR, the setting time of the cementitious systems decreases; when the content of CCR is 10%, the initial setting time and the final setting time of the cementitious systems are 190 min and 280 min, and when the content of CCR is 20%, the initial setting time and the final setting time of the cementitious systems are 160 min and 240 min, respectively. The main reason for this is that an increase in CCR content in the cementitious systems of alkaline substances results in an accelerated hydration rate of the material; on the other hand, an increase in CCR content leads to an increase in the water demand of the cementitious systems. These are the two reasons for the shortening of the coagulation time of the cementitious systems. When the content of CCR is 15% and with the content of SS in the cementitious systems changing in the range of 10–30%, the coagulation time of the cementitious systems gradually increases; however, the overall difference is relatively small. The initial setting time is 170 min and the final setting time is approximately 260 min. The main reason for this is that the SS raw material contains a small amount of $\text{Ca}(\text{OH})_2$, increasing the alkalinity of the cementitious systems, making up for the lack of early activity of the SS and the reduction in the content of GBFS.

3.3. Compressive Strength

Figure 5 shows the compressive strength test results of the CCR-GBFS-SS cementitious systems with a change in the curing time with different contents of CCR. Figure 6 shows the compressive strength test results of the CCR-GBFS-SS cementitious systems with a change in the curing time when the content of SS is different. In Figure 5, with a gradual increase in the content of CCR in the cementitious systems, the compressive strength of the cementitious systems at all ages first increases and then decreases. When the content of CCR is 15%, the 28-day compressive strength of CCR-GBFS-SS cementitious systems is the highest, at 41.5 MPa. However, when the CCR content in the cementitious systems changes

in the range of 10–20%, the overall difference in the compressive strength at different ages is very small and the difference in the compressive strength of cementitious systems at all curing ages is less than 10%. This shows that the CCR hydration process is slow; in the hydration reaction process in cementitious systems, the ionisation of OH^- is limited within a certain range to increase the content of CCR. The compressive strength of the cementitious systems will not have a great impact on GBFS–SS cementitious systems, and the activation effect needs to be further improved. In Figure 6, when the content of CCR is 15% and the content of GY is 5%, with a gradual increase in the content of SS, the compressive strength of the cementitious systems shows a downward trend at all ages, especially in the early stage. When the content of SS is 20% and 30%, the 28-day compressive strengths of the cementitious systems are 36.8 MPa and 28.4 MPa, respectively. At 20% SS, the compressive strength was 11.3% lower than that at 10% SS, and at 30% SS, the compressive strength was 31.6% lower than that at 10%, suggesting that a moderate amount of SS contributes to the compressive strength of cementitious systems with longer curing times. This is mainly due to the extension of the curing time, during which SS began to gradually hydrate, producing a small amount of $\text{Ca}(\text{OH})_2$ and C-S-H gel [15]. The compressive strength of the cementitious systems plays a certain role in improving the compressive strength; however, the effect of SS on the compressive strength of cementitious systems is smaller than that of the GBFS hydration reaction. When coupled with the limited activation effect of CCR, when the SS content is 30%, the compressive strength of cementitious systems in the later stage still exhibits a relatively large decline.

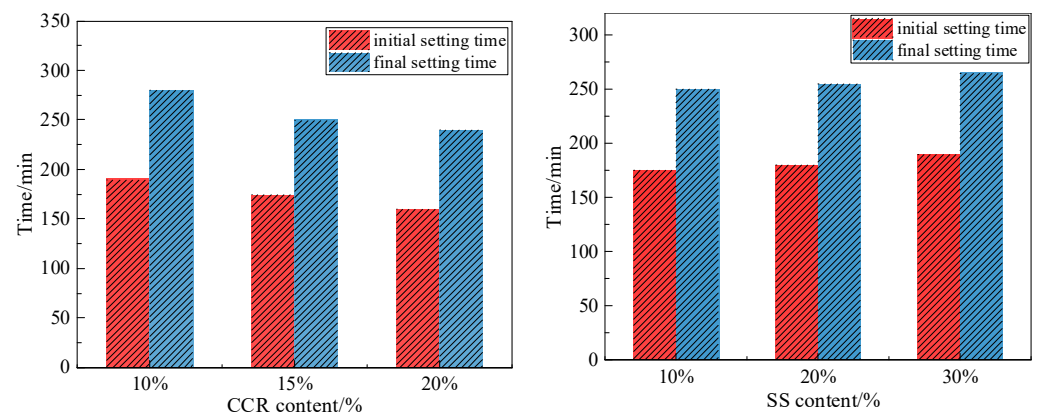


Figure 4. Setting time of cementitious materials with different material contents.

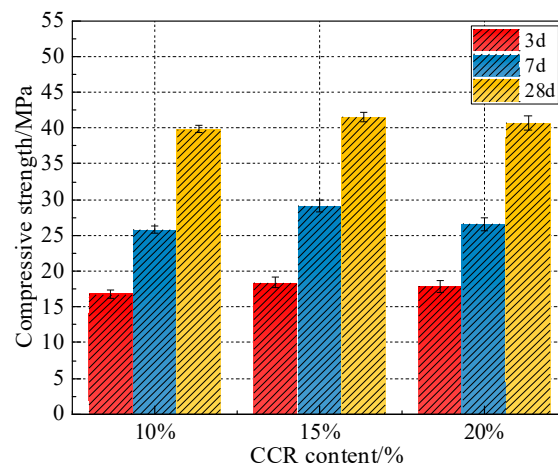


Figure 5. Compressive strength of cementitious systems with different CCR content.

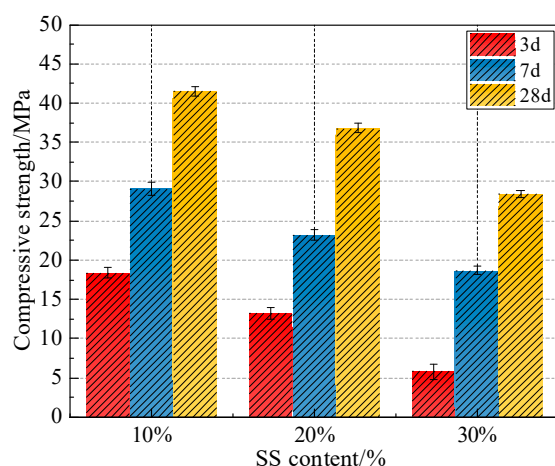


Figure 6. Compressive strength of cementitious systems with different SS contents.

4. Hydration Characteristics of CCR-GBFS-SS Cementitious Systems

In order to further study the mechanism of action of CCR-GBFS-SS cementitious systems, a 15% CCR content, 10% SS content, 70% GBFS content and 5% GY content were selected to prepare cementitious materials. Hydration was terminated at 3d, 7d, and 28d; microscopic tests were carried out and the results were analysed.

4.1. Hydration Products and Chemical Structure of Cementitious Systems at Different Curing Ages

Figure 7 shows the XRD curve of CCR-GBFS-SS cementitious systems at different curing ages. In Figure 7, the main hydration product of the cementitious systems at different ages is the amorphous mineral, ettringite. In addition to this, the cementitious systems also contain residual RO phases (MgO, FeO, MnO) from the raw materials, $\text{Ca}(\text{OH})_2$ and calcite from the carbonation reaction. It has been shown that a large portion of the hydration products of alkali-activated cementitious systems is amorphous gels, which do not have very distinct diffraction peaks in XRD spectra; instead, they exhibit widely diffuse peaks [26,27]. The diffuse peaks in CCR-GBFS-SS cementitious systems are mainly concentrated in $2\theta = 25\text{--}35^\circ$, and are mainly attributed to amorphous C-(A)-S-H gels. C-(A)-S-H gels are formed via the repolymerisation of active silica and active aluminium from GBFS with Ca^{2+} in an alkaline environment; they are an amorphous product and the main source of the compressive strength of cementitious systems [28]. Ettringite is a kind of hydrated calcium-aluminium sulphate generated by elements such as calcium, aluminium and sulphur in cementitious systems and can provide compressive strength for cementitious systems at the initial stage of the hydration reaction. It is beneficial to the development of the mechanical properties of cementitious systems [29]. The gradual weakening of the $\text{Ca}(\text{OH})_2$ diffraction peaks in the cementitious systems indicates that the CCR in the cementitious systems is gradually consumed with the prolongation of the age of curing, promoting the pozzolanic reaction and the hydration of the GBFS in the cementitious systems, as well as the formation of hydration products. There is a calcite diffraction peak in the cementitious systems, and this is due to the hydration of CCR and SS to generate $\text{Ca}(\text{OH})_2$ and the carbonation reaction with CO_2 in the air during the preparation and curing of the cementitious systems. The formation of calcite in the cementitious systems will promote the formation of C-(A)-S-H gel and improve the compressive strength [30,31].

The FT-IR spectra for the CCR-GBFS-SS cementitious systems are shown in Figure 8. In Figure 8, there is an absorption peak at 3640 cm^{-1} for the CCR-GBFS-SS cementitious systems, representing O-H expansion and contraction vibrations in $\text{Ca}(\text{OH})_2$ [32,33]. With the gradual prolongation of the age of curing, the absorption peak here is gradually weakened, and combined with the XRD test results, this shows that, with the prolongation of the age of curing of the cementitious systems, CCR is more involved in the pozzolanic

reaction and its content is gradually reduced. The absorption peaks near 3420 cm^{-1} and 1650 cm^{-1} are mainly H-O-H bond stretching vibrations and bending vibrations [34,35], respectively, mainly caused by the hydroxyl group of crystalline water in the cementitious systems, and it can be seen from the figure that the 3442 cm^{-1} and 1650 cm^{-1} peaks decreased substantially with the increase in the age of curing, which is consistent with the literature [36]. The spectral band near 1420 cm^{-1} is caused by the vibration of C-O bonds in calcite [37]; it is mainly generated due to the hydration of CCR and SS in the raw material to generate $\text{Ca}(\text{OH})_2$ and the carbonation reaction with air. The peaks gradually increase with the hydration time, and this shows that more carbonates are generated in the cementitious systems, agreeing with the XRD analysis results. The absorption peak near 870 cm^{-1} is caused by the stretching vibrations of Al-O-H groups [38], indicating that the aluminium phases in GBFS and SS in the cementitious systems are consumed in large quantities and participate in the reaction to produce a large amount of ettringite and C-A-S-H gels. The vibrations in the cementitious systems at around 1110 cm^{-1} are related to the bending and stretching vibrations of S-O in the structure of ettringite and GY [33,39], suggesting that ettringite is generated in the cementitious systems. The broad absorption bands appearing at around 960 cm^{-1} and 450 cm^{-1} are caused by the bending vibrations in the Si-O and Si-O-Si on the surface [40,41], and are characteristic spectral bands of C-(A)-S-H gels.

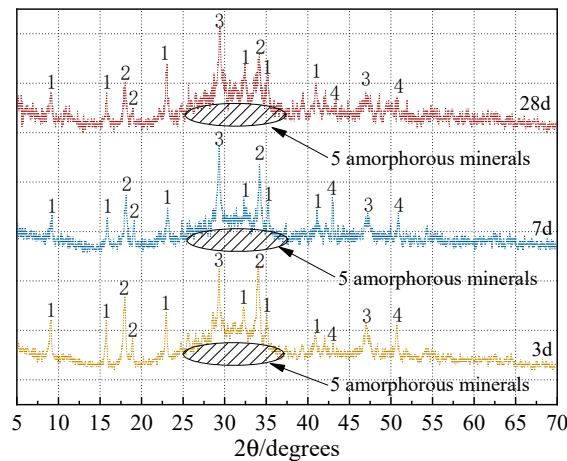


Figure 7. XRD of cementitious systems at different curing ages. 1-Ettringite, 2- $\text{Ca}(\text{OH})_2$, 3- CaCO_3 , 4-RO, 5-C-(A)-S-H gels.

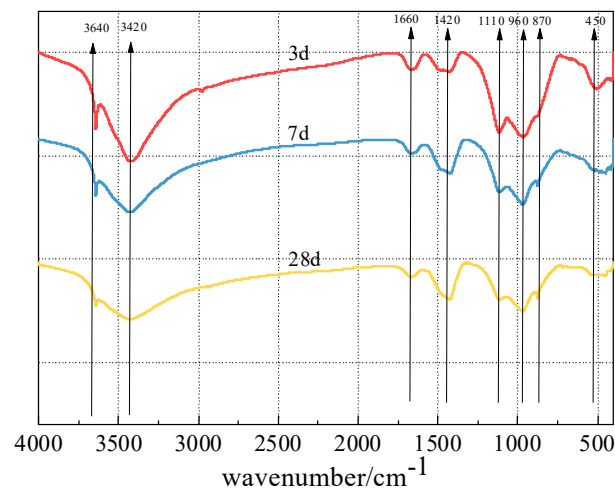


Figure 8. FT-IR curves of cementitious systems at different curing ages.

4.2. Thermal Analysis of Cementitious Systems under Different Curing Ages

Figure 9 shows the TG curves and DTG curves of CCR-GBFS-SS cementitious systems after 3 days and 28 days. From the DTG curves, it can be seen that there are four obvious weight loss peaks in the cementitious systems at different curing ages, and they are located at 50–200 °C, 400–500 °C, 700–800 °C and 900–1000 °C. The peak at 50–200 °C is the weight loss of the cementitious systems due to the dehydration of ettringite and C-(A)-S-H gels [42]. The peak at 400–500 °C is the weight loss peak from thermal decomposition of $\text{Ca}(\text{OH})_2$ in the cementitious systems [43]. The peak at 600–1000 °C is due to the thermal decomposition of calcite in the cementitious systems [44]. From the TG curves, it can be derived that curing the cementitious systems for 3 days and 28 days at 50–200 °C results in a mass loss of 9.32% and 12.50%, respectively. This shows that with the increase in the age of curing, the ettringite and C-(A)-S-H gel in the cementitious systems increased by 34.12%. The ettringite and C-(A)-S-H gel are the main sources of the compressive strength of cementitious systems. These results are consistent with the XRD analysis results of the cementitious systems and also corroborate with the compressive strength of the cementitious systems. The weight loss of $\text{Ca}(\text{OH})_2$ in the cementitious systems at 3 and 28 days was 1.95% and 1.43%, respectively, which showed that the amount of $\text{Ca}(\text{OH})_2$ in the cementitious systems gradually decreased with the increase in the age of curing. This is consistent with the XRD and FT-IR analyses, indicating that the CCR in the cementitious systems was consumed in the pozzolanic reaction. The weight loss at 600–1000 °C was 5.07% and 5.12%, respectively. With the increase in the curing age, the content of CaCO_3 in the cementitious systems increased slightly, consistent with XRD and FT-IR analyses, showing that there was a slow carbonization reaction in the cementitious systems.

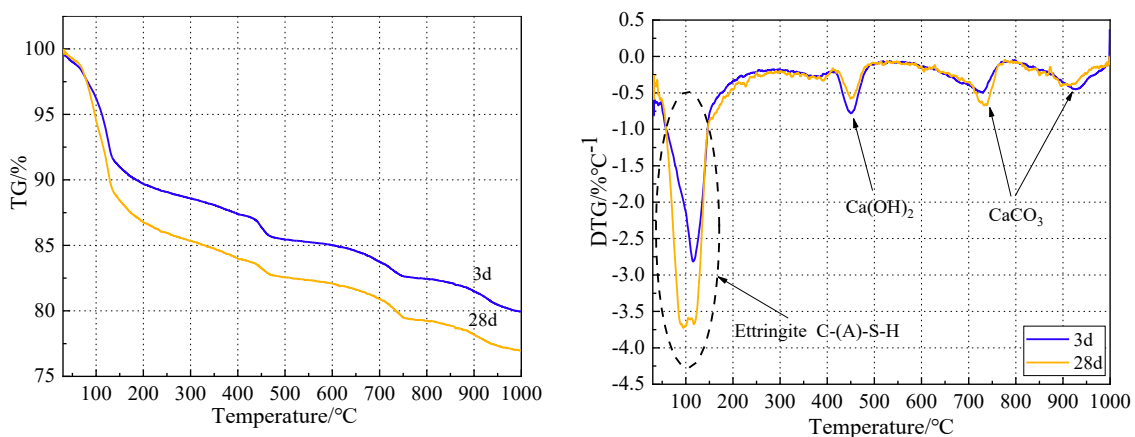


Figure 9. TG-DTG curves of cementitious systems at different curing ages.

4.3. Micro-Morphology of Cementitious Systems at Different Curing Ages

Figure 10 shows the microscopic morphology of the CCR-GBFS-SS cementitious systems at different curing ages. In Figure 10, with the gradual extension of the curing time (3, 7 and 28 days), the degree of hydration of the cementitious systems increases. When the CCR-GBFS-SS cementitious systems are cured for 3 days, the microstructure of the cementitious system matrix is relatively loose, and a large amount of stout ettringite and a small amount of C-(A)-S-H gel can be seen on the surface of the cementitious system matrix, clustered with each other, providing the main early compressive strength for the cementitious systems. This is in line with the microanalyses via XRD and FT-IR and other microanalyses. From the microscopic morphology of the cementitious systems cured for 7 days, it can be seen that the amount of ettringite in the cementitious systems gradually increases, the needle and rod-like ettringite was arranged more closely, the amount of honeycomb C-(A)-S-H gel in the cementitious systems gradually increased and the ettringite and the C-(A)-S-H gel overlapped to form a dense spatial structure, further improving the compressive strength of the cementitious systems. In cementitious

systems cured for 28 days, C-(A)-S-H gel generation continues to increase and the hydration products are more closely connected. A spatially dense three-dimensional honeycomb structure is formed, playing a skeleton support role in the cementitious systems. The matrix in these cementitious systems is denser than in the early stage, and this is reflected in the macro-mechanical properties of the specimens, with a higher compressive strength at 28 days. On the other hand, the generation of calcite in the cementitious systems cured for 28 days continues to increase, and this is consistent with the results of XRD, FT-IR, and TG-DTG analyses. The calcite in the cementitious systems can also play a role in refining the pore space and enhancing the densification of the matrix of the cementitious systems.

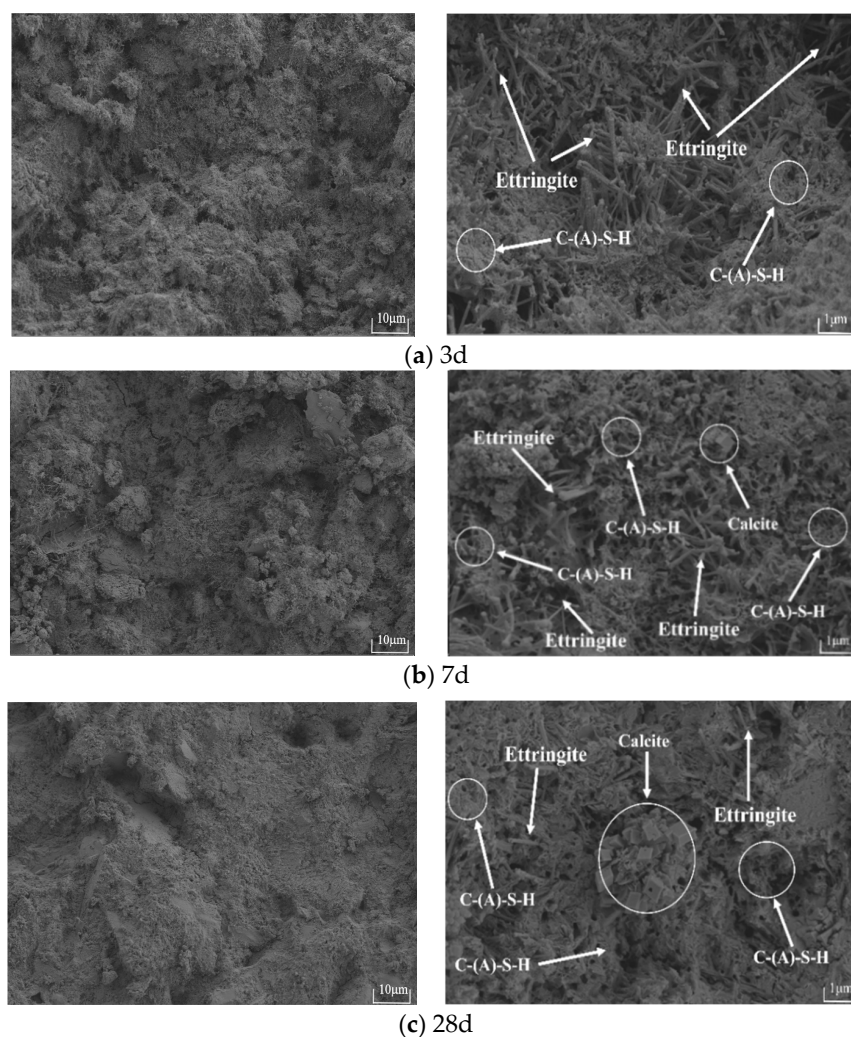


Figure 10. Micro-morphology of cementitious systems at different curing ages.

5. Discussion on the Mechanism of CCR-GBFS-SS Cementitious Systems

In the CCR-GBFS-SS cementitious systems studied in this paper, CCR is the main alkaline activator, GBFS and SS are the main precursors, and a small amount of GY is used as a salt activator to supplement the cementitious systems with an appropriate amount of sulphate. GBFS is mainly composed of glass, and the main structural units of the glass body are silica tetrahedrons, with a strong chemical activity, and a small amount of alumina tetrahedrons. There is also a small amount of aluminosilicate microcrystals with an extremely low crystallinity. Mixing CCR, SS, GBFS and GY after grinding them finely to prepare non-cement-based multi-solid waste cementitious systems leads to each of them playing a synergistic role. As shown in the previous section, XRD, FT-IR, TG-DTG and other tests can determine the hydration products in CCR-GBFS-SS cementitious systems; the synergistic effect in the cementitious systems is mainly reflected in the following.

In the hydration and hardening processes of CCR-GBFS-SS cementitious systems, CCR takes the lead in ionising Ca^{2+} and OH^- , GY ionises Ca^{2+} and SO_4^{2-} , and the GBFS vitreous particles are activated to decompose and depolymerise under the dual action of OH^- and SO_4^{2-} in the cementitious systems. The Ca-O bonds, Si-O bonds and Al-O bonds are fractured one after another, releasing a large amount of Ca^{2+} as well as a small amount of OH^- . In an alkaline environment, the hydration reactions of the fractured Si-O-Si and Si-O-Al bonds in the GBFS with OH^- and H_2O in the cementitious systems produce $[\text{H}_3\text{AlO}_4]^{2-}$ as well as $[\text{H}_3\text{SiO}_4]^-$ [26,27]. With this hydration, CCR and GY are constantly consumed, prompting the SS to carry out hydration reactions. In an alkaline environment, the SS in the C_2S and C_3S gradually decomposes, generating C-S-H gel, Ca^{2+} and OH^- , which is involved in the hydration reaction. Further stabilisation of the pH value of the cementitious systems and the late strength of the cementitious systems also have a certain role in promoting these reactions. The CCR-GBFS-SS cementitious systems contain a large amount of Ca^{2+} , OH^- , $[\text{H}_3\text{AlO}_4]^{2-}$ and $[\text{H}_3\text{SiO}_4]^-$, and GY ionises SO_4^{2-} with different degrees of polymerisation to generate C-(A)-S-H gels and ettringite. Cementation of GBFS and SS forms a spatially dense, three-dimensional honeycomb structure to provide the main strength of the cementitious systems.

In addition, from the XRD, FT-IR, TG-DTG and SEM microscopic analyses, it can be seen that, with the increase in the curing time, the hydration reaction gradually increases. The ettringite is mainly generated in the early stage, promoting the development of the early strength of cementitious systems. The SS participates in the hydration reaction in the late stage of hydration, and appropriate SS contents have a certain enhancing effect on the late compressive strength of cementitious systems. There is a gradual increase in C-(A)-S-H gel generation in the cementitious systems, providing a steady strength increase to the cementitious systems. As the cementitious systems use CCR as the main activator, it is easy for carbonation reactions to occur during the curing process, and the generated calcite will also play a role in refining the pore space and increasing the number of nucleation sites for hydration products [45]. The alkalinity of the aqueous solutions of cementitious CCR-GBFS-SS systems is low, especially in the early stage. When a mixture of 15% CCR, 10% SS, 70% GBFS and 5% GY is adopted, the compressive strength of the cementitious systems in 3 days is 46.5% of that in 28 days, and the growth in the compressive strength of the cementitious systems is slow. Figure 11 shows the early appearance of a specimen of a CCR-GBFS-SS cementitious system and in this section in Figure 11, it can be seen that there are obvious differences in the appearance of CCR-GBFS-SS cementitious systems and Portland cement net mortar specimens regarding the milky white colour. When the content of SS is large, the early section of the specimen of CCR-GBFS-SS cementitious systems is mostly grey and part of the visible section is dark green. The use of NaOH and other strong bases to stimulate the GBFS-SS cementitious systems leads to this dark green colour. It is shown that the activation of GBFS-SS cementitious systems using CCR is less effective than that of strong alkali activation, and CCR has a slow effect on GBFS-SS cementitious system activation.

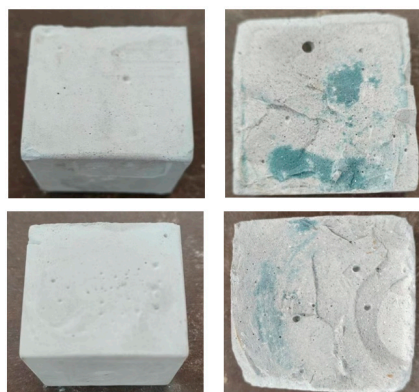


Figure 11. Appearance and section of cementitious material.

Combined with the above discussion of the mechanism, the main hydration process of CCR-GBFS-SS cementitious systems is shown in Figure 12.

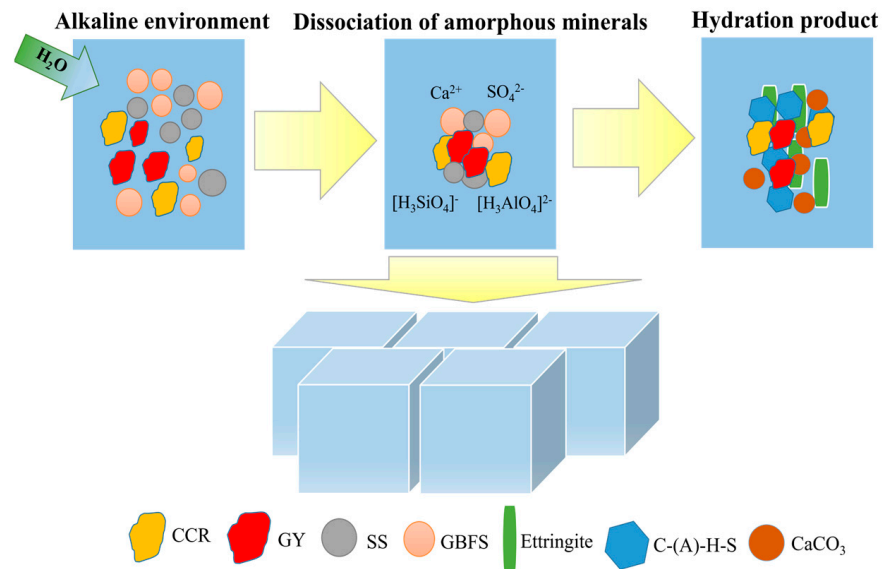


Figure 12. Hydration mechanism of CCR-GBFS-SS cementitious systems.

6. Conclusions

In this paper, CCR, SS, GBFS and GY are used to prepare CCR-GBFS-SS multi-solid cementitious materials, and the effect of the CCR content and SS content on the compressive strength of the cementitious systems is discussed. The hydration products are analysed, alongside the chemical structure and microscopic morphology of the CCR-GBFS-SS cementitious systems, and the hydration mechanism of CCR-GBFS-SS cementitious systems is summarized. This paper can be used to provide a reference for the elimination of CCR and other low-value solid wastes, as well as for the preparation of multi-solid, low-carbon cementitious materials. This paper has the following main conclusions:

1. CCR can be used in binary GBFS-SS alkali-activated cementitious systems as an alkaline activator. Cementitious systems can be controlled by the time of coagulation; however, the liquidity performance is poor. The cementitious systems' 28-day compressive strength was up to 41.5 Mpa, but the influence of CCR on the cementitious systems' alkalinity is limited. When the content of CCR in the cementitious systems varied from 10–20%, there was no significant effect on the compressive strength at all ages. SS contributes to the late compressive strength of the cementitious system and has a lesser effect on the late compressive strength when its content is 20%. The content of SS in CCR-GBFS-SS cementitious systems should not be too high.
2. In CCR-GBFS-SS cementitious systems, with an increase in the curing time, CCR is gradually consumed, which promotes the continuation of pozzolanic reactions of GBFS in the cementitious systems, and the number of hydration products in the cementitious systems gradually increases, changing the matrix of cementitious systems from loose to dense.
3. The presence of CCR in CCR-GBFS-SS cementitious systems maintains the alkaline environment. SS can provide alkaline substances such as calcium and magnesium, GBFS can provide activated silicon and activated aluminium and gypsum can provide SO_4^{2-} . These four compounds work together to form hydration products such as C-(A)-S-H gels and ettringite. The compressive strength of the cementitious systems is mainly derived from the three-dimensional network structure formed by the C-(A)-S-H gels and ettringite.

Author Contributions: Conceptualisation, methodology, investigation, formal analysis, Q.W. Writing—review and editing, conceptualisation, methodology, investigation, data curation, writing—original draft preparation, Y.W. Conceptualization, methodology, investigation, formal analysis, writing—review and editing, X.G. Conceptualization, methodology, J.L. Conceptualization, methodology, X.X. All authors have read and agreed to the published version of the manuscript.

Funding: The authors are very grateful for the support from the following funds: National Key Research and Development Program of China (No.2023YFC3904303), National Natural Science Foundation of China (No.52234004) and the Science and Technology Plan Project of Shenyang (22-322-3-02).

Data Availability Statement: The raw data supporting the conclusions of this article will be made available by the authors on request.

Conflicts of Interest: The authors declare that they have no known competing financial interests or personal relationships that could have appeared to influence the work reported in this paper.

References

1. Juenger, M.C.G.; Winnefeld, F.; Provis, J.L.; Ideker, J.H. Advances in alternative cementitious binders. *Cem. Concr. Res.* **2011**, *41*, 1232–1243. [[CrossRef](#)]
2. Provis, J.L.; Palomo, A.; Shi, C. Advances in understanding alkali-activated materials. *Cem. Concr. Res.* **2015**, *78*, 110–125. [[CrossRef](#)]
3. Ng, C.; Alengaram, U.J.; Wong, L.S.; Mo, K.H.; Jumaat, M.Z.; Ramesh, S. A review on microstructural study and compressive strength of geopolymer mortar, paste and concrete. *Constr. Build. Mater.* **2018**, *186*, 550–576. [[CrossRef](#)]
4. Hassan, A.; Arif, M.; Shariq, M. Use of geopolymer concrete for a cleaner and sustainable environment—A review of mechanical properties and microstructure. *J. Clean. Prod.* **2019**, *223*, 704–728. [[CrossRef](#)]
5. Luukkonen, T.; Abdollahnejad, Z.; Yliniemi, J.; Kinnunen, P.; Illikainen, M. One-part alkali-activated materials: A review. *Cem. Concr. Res.* **2018**, *103*, 21–34. [[CrossRef](#)]
6. Amran, Y.M.; Alyousef, R.; Alabduljabbar, H.; El-Zeadani, M. Clean production and properties of geopolymer concrete; A review. *J. Clean. Prod.* **2020**, *251*, 119679. [[CrossRef](#)]
7. Yang, T.; Gao, X.; Zhang, J.; Zhuang, X.; Wang, H.; Zhang, Z. Sulphate resistance of one-part geopolymer synthesized by calcium carbide residue-sodium carbonate-activation of slag. *Compos. Part B Eng.* **2022**, *242*, 110024. [[CrossRef](#)]
8. Li, W.; Yi, Y. Use of carbide slag from acetylene industry for activation of ground granulated blast-furnace slag. *Constr. Build. Mater.* **2020**, *238*, 117713. [[CrossRef](#)]
9. Zhang, J.; Tan, H.; He, X.; Yang, W.; Deng, X. Utilization of carbide slag-granulated blast furnace slag system by wet grinding as low carbon cementitious materials. *Constr. Build. Mater.* **2020**, *249*, 118763. [[CrossRef](#)]
10. Dueramae, S.; Tangchirapat, W.; Sukontasukkul, P.; Chindaprasirt, P.; Jaturapitakkul, C. Investigation of compressive strength and microstructures of activated cement free binder from fly ash-calcium carbide residue mixture. *J. Mater. Res. Technol.* **2019**, *8*, 4757–4765. [[CrossRef](#)]
11. Namarak, C.; Satching, P.; Tangchirapat, W.; Jaturapitakkul, C. Improving the compressive strength of mortar from a binder of fly ash-calcium carbide residue. *Constr. Build. Mater.* **2017**, *147*, 713–719. [[CrossRef](#)]
12. Guo, W.; Zhao, Q.; Sun, Y.; Xue, C.; Bai, Y.; Shi, Y. Effects of various curing methods on the compressive strength and microstructure of blast furnace slag-fly ash-based cementitious material activated by alkaline solid wastes. *Constr. Build. Mater.* **2022**, *357*, 129397. [[CrossRef](#)]
13. Guo, W.; Zhang, Z.; Bai, Y.; Zhao, G.; Sang, Z.; Zhao, Q. Development and characterization of a new multi-strength level binder system using soda residue-carbide slag as composite activator. *Constr. Build. Mater.* **2021**, *291*, 123367. [[CrossRef](#)]
14. Zhang, S.; Niu, D. Hydration and mechanical properties of cement-steel slag system incorporating different activators. *Constr. Build. Mater.* **2023**, *363*, 129981. [[CrossRef](#)]
15. Zhao, J.; Li, Z.; Wang, D.; Yan, P.; Luo, L.; Zhang, H.; Zhang, H.; Gu, X. Hydration superposition effect and mechanism of steel slag powder and granulated blast furnace slag powder. *Constr. Build. Mater.* **2023**, *366*, 130101. [[CrossRef](#)]
16. Ma, Y.; Zhang, B.; Wang, B.; Lin, X.; Zhu, J.; Huang, P.; Ji, T. Fluidity, mechanical properties, shrinkage of alkali-activated slag/stainless steel slag mortars with composite activators. *J. Build. Eng.* **2023**, *75*, 106877. [[CrossRef](#)]
17. Zhong, J.; Cao, L.; Li, M.; Wang, S.; Liu, F.; Lv, X.; Peng, X. Mechanical properties and durability of alkali-activated steel slag-blastfurnace slag cement. *J. Iron Steel Res. Int.* **2023**, *30*, 1342–1355. [[CrossRef](#)]
18. Ghorbani, S.; Stefanini, L.; Sun, Y.; Walkley, B.; Provis, J.L.; De Schutter, G.; Matthys, S. Characterisation of alkali-activated stainless steel slag and blast-furnace slag cements. *Cem. Concr. Compos.* **2023**, *143*, 105230. [[CrossRef](#)]
19. Li, W.; Ma, S.; Zhang, S.; Shen, X. Physical and chemical studies on cement containing sugarcane molasses. *J. Therm. Anal. Calorim.* **2014**, *118*, 83–91.
20. GB/T 8077-2012; Methods for Testing Uniformity of Concrete Admixture. China National Standardization Administration Committee: Beijing, China, 2012.

21. Wang, Y.; Tan, H.; Gu, X.; He, X.; Zhang, J. Preparation of nano-kaolin by wet-grinding process and its application as accelerator in Portland cement. *J. Build. Eng.* **2021**, *44*, 103401. [[CrossRef](#)]
22. GB/T 1346-2011; Test Methods for Water Requirement of Normal Consistency, Setting Time and Soundness of the Portland Cement. China National Standardization Administration Committee: Beijing, China, 2011.
23. Zhang, C.; Chen, M.; Liu, R.; Li, X.; Yan, J.; Zhu, Z.; Fan, F. Synergistic effect of PVA fiber and PTB emulsion on mechanical properties of cementitious composites for damage repair in operating tunnels. *KSCE J. Civ. Eng.* **2022**, *26*, 5222–5239. [[CrossRef](#)]
24. GB/T 17671-2021; Test Method of Cement Mortar Strength (ISO Method). China National Standardization Administration Committee: Beijing, China, 2021.
25. Wu, M.; Zhang, Y.; Liu, G.; Wu, Z.; Yang, Y.; Sun, W. Experimental study on the performance of lime-based low carbon cementitious materials. *Constr. Build. Mater.* **2018**, *168*, 780–793. [[CrossRef](#)]
26. Zhang, W.; Hao, X.; Wei, C.; Zeng, Q.; Ma, S.; Liu, X.; Zhang, Z.; Webeck, E. Synergistic enhancement of converter steelmaking slag, blast furnace slag, Bayer red mud in cementitious materials: Strength, phase composition, and microstructure. *J. Build. Eng.* **2022**, *60*, 105177. [[CrossRef](#)]
27. Zhang, W.; Liu, X.; Zhang, Z.; Li, Y.; Gu, J. Synergic effects of circulating fluidized bed fly ash-red mud-blast furnace slag in green cementitious materials: Hydration products and environmental performance. *J. Build. Eng.* **2022**, *58*, 105007. [[CrossRef](#)]
28. Hanjitsuwan, S.; Phoo-Ngernkham, T.; Li, L.-Y.; Damrongwiriyanupap, N.; Chindaprasirt, P. Strength development and durability of alkali-activated fly ash mortar with calcium carbide residue as additive. *Constr. Build. Mater.* **2018**, *162*, 714–723. [[CrossRef](#)]
29. Wang, Y.; Liu, X.; Zhu, X.; Zhu, W.; Yue, J. Synergistic effect of red mud, desulfurized gypsum and fly ash in cementitious materials: Mechanical performances and microstructure. *Constr. Build. Mater.* **2023**, *404*, 133302. [[CrossRef](#)]
30. Wang, J.; Lyu, X.; Wang, L.; Cao, X.; Liu, Q.; Zang, H. Influence of the combination of calcium oxide and sodium carbonate on the hydration reactivity of alkali-activated slag binders. *J. Clean. Prod.* **2018**, *171*, 622–629. [[CrossRef](#)]
31. Burciaga-Díaz, O.; Betancourt-Castillo, I.E.; Montes-Escobedo, M.E.; Escalante-García, J.I. One-part pastes and mortars of CaO-Na₂CO₃ activated blast furnace slag: Microstructural evolution, cost and CO₂ emissions. *Constr. Build. Mater.* **2023**, *368*, 130431. [[CrossRef](#)]
32. Li, J.; Chen, M.; Jin, X.; Chen, Y.; Dai, Z.; Ou, Z.; Tang, Q. Calibration of a multiple axes 3-D laser scanning system consisting of robot, portable laser scanner and turntable. *Optik* **2011**, *122*, 324–329. [[CrossRef](#)]
33. Wu, M.; Zhang, Y.; Jia, Y.; She, W.; Liu, G.; Yang, Z.; Zhang, Y.; Zhang, W.; Sun, W. Effects of sodium sulfate on the hydration and properties of lime-based low carbon cementitious materials. *J. Clean. Prod.* **2019**, *220*, 677–687. [[CrossRef](#)]
34. Hao, X.; Liu, X.; Zhang, Z.; Zhang, W.; Lu, Y.; Wang, Y.; Yang, T. In-depth insight into the cementitious synergistic effect of steel slag and red mud on the properties of composite cementitious materials. *J. Build. Eng.* **2022**, *52*, 104449. [[CrossRef](#)]
35. Shao, J.; Gao, J.; Zhao, Y.; Chen, X. Study on the pozzolanic reaction of clay brick powder in blended cement pastes. *Constr. Build. Mater.* **2019**, *213*, 209–215. [[CrossRef](#)]
36. Cong, P.; Cheng, Y.; Ge, W.; Zhang, A. Mechanical, microstructure and reaction process of calcium carbide slag-waste red brick powder based alkali-activated materials (CWAAMs). *J. Clean. Prod.* **2021**, *331*, 129845. [[CrossRef](#)]
37. Bai, Y.; Guo, W.; Zhang, Y.; Xue, C.; Xu, Z.; Gao, Q.; Xiao, C.; Zhao, Q. Low carbon binder preparation from slag-red mud activated by MSWI fly ash-carbide slag: Hydration characteristics and heavy metals' solidification behavior. *J. Clean. Prod.* **2022**, *374*, 134007. [[CrossRef](#)]
38. Scholtzová, E.; Kucková, L.; Kožíšek, J.; Tunega, D. Structural and spectroscopic characterization of ettringite mineral-combined DFT and experimental study. *J. Mol. Struct.* **2015**, *1100*, 215–224. [[CrossRef](#)]
39. Ch, L.; Meng, W.; Xiao, L. Working performance of red mud-based grouting materials mixed with ultrafine limestone and quartz. *Constr. Build. Mater.* **2023**, *383*, 131326. [[CrossRef](#)]
40. Zhang, N.; Li, H.; Peng, D.; Liu, X. Properties evaluation of silica-alumina based concrete: Durability and environmental friendly performance. *Constr. Build. Mater.* **2016**, *115*, 105–113. [[CrossRef](#)]
41. Xu, C.; Ni, W.; Li, K.; Zhang, S.; Xu, D. Activation mechanisms of three types of industrial by-product gypsums on steel slag-granulated blast furnace slag-based binders. *Constr. Build. Mater.* **2021**, *288*, 123111. [[CrossRef](#)]
42. Zhou, J.; Zheng, K.; Liu, Z.; Chen, L.; Lippiatt, N. Use of gamma-Al₂O₃ to prevent alkali-silica reaction by altering solid and aqueous compositions of hydrated cement paste. *Cem. Concr. Res.* **2019**, *124*, 105817. [[CrossRef](#)]
43. Monteagudo, S.; Moragues, A.; Gálvez, J.; Casati, M.; Reyes, E. The degree of hydration assessment of blended cement pastes by differential thermal and thermogravimetric analysis. Morphological evolution of the solid phases. *Thermochim. Acta* **2014**, *592*, 37–51. [[CrossRef](#)]
44. Duan, S.; Liao, H.; Cheng, F.; Song, H.; Yang, H. Investigation into the synergistic effects in hydrated gelling systems containing fly ash, desulfurization gypsum and steel slag. *Constr. Build. Mater.* **2018**, *187*, 1113–1120. [[CrossRef](#)]
45. Oderji, S.Y.; Chen, B.; Shakya, C.; Ahmad, M.R.; Shah, S.F.A. Influence of superplasticizers and retarders on the workability and strength of one-part alkali-activated fly ash/slag binders cured at room temperature. *Constr. Build. Mater.* **2019**, *229*, 116891. [[CrossRef](#)]

Disclaimer/Publisher's Note: The statements, opinions and data contained in all publications are solely those of the individual author(s) and contributor(s) and not of MDPI and/or the editor(s). MDPI and/or the editor(s) disclaim responsibility for any injury to people or property resulting from any ideas, methods, instructions or products referred to in the content.